European Journal of Medicinal Chemistry 175 (2019) 107–113

Contents lists available at ScienceDirect

European Journal of Medicinal Chemistry

journal homepage: http://www.elsevier.com/locate/ejmech

Research paper

Ligand retargeting by binding site analogy

Lars Wiedmer [a], Claude Schärer [b], Dimitrios Spiliotopoulos [a], Marianne Hürzeler [b], Paweł Śledź [a], Amedeo Caflisch [a, *]

[a] Department of Biochemistry, University of Zurich, Winterthurerstrasse 190, CH-8057, Zurich, Switzerland
[b] University of Applied Sciences and Arts Northwestern Switzerland, Hofackerstrasse 30, CH-4132, Muttenz, Switzerland

ARTICLE INFO

Article history:
Received 18 March 2019
Received in revised form
11 April 2019
Accepted 13 April 2019
Available online 25 April 2019

Keywords:
MTH1
Retargeting
Docking
Molecular dynamics
Protein X-ray crystallography
Aspartic protease

ABSTRACT

The DNA-repair enzyme MutT homolog 1 (MTH1) is a potential target for a broad range of tumors. Its substrate binding site features a non-catalytical pair of aspartic acids which resembles the catalytic dyad of aspartic proteases. We hypothesized that inhibitors of the latter might be re-targeted for MTH1 despite the two enzyme classes having different substrates and catalyze different reactions. We selected from the crystal structures of holo aspartic proteases a library of nearly 350 inhibitors for *in silico* screening. Three fragment hits were identified by docking and scoring according to a force field-based energy with continuum dielectric solvation. These fragments showed good ligand efficiency in a colorimetric assay (MW <300 Da and $IC_{50}<50$ μM). Molecular dynamics simulations were carried out for determining the most favorable interaction patterns. On the basis of the simulation results we evaluated *in vitro* seven commercially available compounds, two of which showed submicromolar potency for MTH1. To obtain definitive evidence of the predicted binding modes we solved the crystal structures of five of the 10 inhibitors predicted *in silico*. The final step of hit optimization was guided by protein crystallography and involved the synthesis of a single compound, the lead **11**, which shows nanomolar affinity for MTH1 in two orthogonal binding assays, and selectivity higher than 2000-fold against its original target (BACE1). The high rate of fragment-hit identification and the fast optimization suggest that ligand retargeting by binding site analogy is an efficient strategy for drug design.

1. Introduction

The human MutT Homolog 1 (MTH1) is part of the DNA repair system in which it hydrolyzes free oxidized nucleotides, particularly 8-oxodGTP and 2-OH-dATP [1]. The phosphate hydrolysis prevents their misincorporations into DNA which otherwise would cause mutations. Thus, MTH1 inhibitors have potential as anticancer drugs. Several groups have reported the identification of high nanomolar MTH1 inhibitors by *in vitro* [2–4] and *in silico* [5] approaches. To date, only a few low nanomolar binders have been reported. The low nanomolar MTH1 inhibitors, TH588 and (S)-crizotinib, showed cytotoxic effects in solid tumor cell lines derived from colorectal, lung, breast, cervical, pancreatic, ovarian, and bone cancers [6,7]. Recent studies have provided strong evidence that potent MTH1 inhibitors do not possess antiproliferative activity which suggests that the cytotoxic effect of TH588 and (S)-crizotinib is due to binding to other targets [8,9]. Therefore, new MTH1 inhibitors can be used to further assess the role of this DNA repair enzyme in cancer cells.

Structurally, MTH1 has the common Nudix hydrolase fold consisting of a β-sheet and α-helices on each side [10]. The modified nucleotides bind to the substrate binding site such that the pyrimidine moiety of the base interacts with two aspartate residues which are adjacent in sequence and three-dimensional space (Asp119, Asp120). The Asp-Asp motif (called also aspartate pair hereafter) in MTH1 is not involved directly in catalysis. Yet, it is reminiscent of the catalytic dyad in the active site of aspartic proteases. A large number of crystal structures of aspartic proteases in the complex with small-molecule ligands is available in the Protein Data Bank [11] because of the importance of these enzymes in human diseases. In particular, BACE, renin, cathepsin D, and plasmepsins, are involved in Alzheimer's disease, hypertension, cancer, and malaria, respectively [12,13].

Here, we hypothesized that structural analogy between the binding site of the target enzyme (MTH1) and functionally unrelated enzymes (aspartic proteases) can be exploited for hit

* Corresponding author. University of Zurich, Switzerland
E-mail address: caflisch@bioc.uzh.ch (A. Caflisch).

https://doi.org/10.1016/j.ejmech.2019.04.037
0223-5234/

identification. More precisely, due to the presence of an aspartate pair in the substrate binding site of both MTH1 and aspartic proteases, small molecule ligands of the latter constitute a privileged library for (medium-throughput) screening of MTH1 ligands. Our hypothesis is inspired by the concept of 'binding site centric chemical space', which implies that binding sites with similar sterical and/or chemical properties recognize similar functional groups [14–16].

Following our hypothesis we have identified three fragment hits for MTH1 (MW <300 Da, $IC_{50}<50$ μM) by docking a library of 342 inhibitors of aspartic proteases with subsequent biochemical and biophysical characterizations. The hit optimization was guided by molecular dynamics simulations such that only seven molecules were tested *in vitro*. We validated the predicted binding mode of five of the 10 compounds by protein crystallography. Based on the available structural information, we decided to synthesize only one molecule which showed low nanomolar potency and confirmed the structure-based design.

2. Results and discussion

We first present the results of the ligand retargeting strategy. We then discuss hit optimization which was initially based on molecular dynamics simulations and in a second stage supported by crystal structures of holo MTH1. In the following we use the term fragment as our inhibitors of MTH1 have molecular weight smaller than 300 Da.

2.1. Ligand retargeting: from protease inhibitors to MTH1 hits

We compiled a library of inhibitors of aspartic proteases with molecular weight larger than 200 Da, and available crystal structure (269, 3, 67, and 3 ligands of BACE1, BACE2, renin, and cathepsin D, respectively; Fig. S1). We then used rDock [17] to dock this library into the rigid binding site of MTH1 from its complex with (R)-crizotinib (PDB code 4C9W). We selected this structure, instead of the complex with (S)-crizotinib, as it has two orientations of the side chain of Asn33, and one of the two orientations is the same as in the apo structure. Taking into account all possible hydrogen-bond patterns between ligands and Asp-Asp pair [18], we assigned five different protonation states to the Asp-Asp motif. Each protonation state was then treated individually during the docking calculations. About two thirds of the 342 aspartic protease inhibitors were discarded because their top 20 poses did not feature the same interactions with the aspartate pair of MTH1 as in the aspartic protease complex from which they originated. The remaining poses from the five docking campaigns were ranked according to the calculated ligand efficiency. The latter was evaluated as the binding energy (calculated by CHARMM [19] and the CHARMM/CGenFF force field [20,21]) divided by the number of non-hydrogen atoms. Electrostatic solvation effects were approximated by the finite-difference Poisson equation, i.e., in the continuum dielectric model [22,23]. We decided to use the calculated ligand efficiency to favour compounds of small sizes which has two advantages. First, docking results are more accurate for small and (mainly) rigid fragments than large and flexible molecules [23–25]. Second, fragments are usually soluble up to the high μM concentration which is useful for the biophysical characterization [26]. Due to availability we tested *in vitro* only three of them, *viz.*, compounds **1**–**3** (Table 1) which ranked 11, 7, and 4, respectively, according to calculated ligand efficiency. The fragment hits **1**–**3**, which originate from the aspartic protease BACE1 (PDB structures 3HW1, 3BUH, and 3MSJ, respectively), showed a potency in the range of 20 μM–50 μM for MTH1 in a colorimetric assay (Fig. S12). Furthermore, hits **1** and **3** show a K_d of 15 μM as measured by isothermal titration calorimetry (ITC) (Fig. S11). Importantly for fragment growing, they have a very favorable ligand efficiency of about 0.40 kcal/mol per non-hydrogen atom and good lipophilic ligand efficiency (Table 1). Furthermore, fragment hits **1** and **3** exhibited 38 and 28 times lower IC_{50} values, respectively, for MTH1 than BACE1. Thus, ligand retargeting by binding site analogy allowed the efficient identification of fragment hits for MTH1.

To further validate the ligand retargeting strategy we tried to solve the crystal structures of MTH1 in complex with the fragment hits **1**–**3**. We were successful for the complex with compound **1** but only at a late stage of the project. More precisely, we identified *in silico* (and tested *in vitro*) compounds **1**–**10** (Tables 1 and 2) before we could solve any crystal structure of holo MTH1. (Note that crystal structures are mentioned here, and not in chronological order, for clarity.) The structural overlap of the binding sites of MTH1 and BACE1 shows that ligand **1** is involved in similar interactions with the aspartate pair in the two enzymes (Fig. 1A). The interactions with Asp119 and Asp32 (in MTH1 and BACE1, respectively) are identical. Furthermore, both Asp120 and Asp228 (in MTH1 and BACE1, respectively) interact with the NH_2 of inhibitor **1** via a water-bridged and direct polar interaction, respectively. The 2-aminoquinoxaline occupies an aromatic cage (Phe72, Trp117, and Phe139) in MTH1 while the corresponding pocket in BACE1 has a single aromatic side chain (Tyr71) and aliphatic side chains (Leu30, Ile118).

We next had to decide which of the hits **1**–**3** would be the most appropriate for optimization. During the *in vitro* validation of our compounds **1**–**3**, a 2-aminoquinazoline derivative was published by others (compound **24** in Ref. 9). This MTH1 inhibitor is similar to our 2-aminoquinoxaline based compound **1**. The hit **2** had slightly worse affinity for MTH1 than compounds **1** and **3**, and is only about five times more potent for MTH1 than BACE1 (Table 1). Furthermore, the purity of compound **2** was only moderate. Given the issues of novelty of hit **1** and limited selectivity of **2**, we decided to focus our hit optimization efforts on fragment **3**, which had favorable ligand efficiency for the MTH1 target, good selectivity against BACE1, and a novel blueprint within the pool of the published inhibitors of MTH1.

We purchased and tested only three analogues of fragment **3**, *viz.*, compounds **4**–**6** (Table 1) because we wanted to investigate three hypotheses, respectively, the dispensability of the propanol and Cl substituents, the role of the NH_2 group, and the influence of a pyridinyl nitrogen as hydrogen bond acceptor. The fragment **4** which lacks the propanol and Cl substituents (on the five-ring and six-ring, respectively) showed similar potency as the hit **3** confirming our hypothesis, based on the docked pose, that these substituents do not contribute to binding. The crystal structure of the complex of MTH1 and fragment **4** provided *a posteriori* validation of our strategy as the binding mode is essentially identical to the one of fragment **3** in BACE1 (Fig. 1B). Concerning the second hypothesis, the docking prediction of the key role of the NH_2 group was validated by the modest potency of fragment **5** which lacks the amino group.

The strong influence of an additional hydrogen bond acceptor, i.e., the nitrogen atom in the pyridinyl ring of compound **6**, was rather unexpected. It resulted in a substantial improvement of potency of compound **6** which showed a 1-μM affinity in both the colorimetric assay and ITC (Table 1). In other words, the replacement of the carbon atom at position 4 of the 2-aminobenzimidazole **4** by a nitrogen resulted in a factor of 40 or 13 higher affinity for compound **6** as measured by the colorimetric assay or ITC, respectively. The overlap of the crystal structures of MTH1 in the complexes with fragments **4** and **6** shows that fragment **6** is more buried and there is an inward rotation of the Asn33 side chain χ_1 angle by about 90° so that the side chain oxygen of Asn33 is in

Table 1
MTH1 hits obtained by docking a library of aspartic protease inhibitors. Dissociation constant (K_d) and half maximal inhibitory concentration (IC_{50}) were measured by ITC and colorimetric assay, respectively. [a]Ligand efficiency (LE) was calculated as $-1.37\log(IC_{50})/HA$, where HA is the number of non-hydrogen atoms. [b]ClogP was calculated by ChemDraw. [c]Lipophilic ligand efficiency (LLE) was calculated as pIC_{50}-ClogP. [d]Values for BACE1 inhibition were taken from previous works [29,32,33], except for fragment **6** which was measured by the assay with the fluorogenic substrate (Fig. S13). The PDB codes of the structures of MTH1 in complex with compounds **1**, **4**, and **6** are 6EQ6, 6EQ5, and, 6EQ2, respectively.

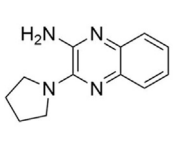

1

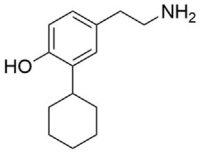

2

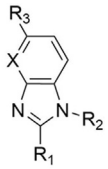

3-6

					MTH1					BACE1	
ID	R1	R2	R3	X	$IC_{50}(\mu M)$	$K_d(\mu M)$	LE[a]	LLE[c]	ClogP[b]	$IC_{50}(\mu M)$	$K_d(\mu M)$
1					23	15	0.40	2.3	2.3	870[d]	
2					46		0.37	1.1	3.2		220[d]
3	NH_2	$(CH_2)_3OH$	C1	C	28	15	0.41	3.2	1.5	770[d]	
4	NH_2			C	44	18	0.60	3.2	1.2		
5				N	123		0.60	3.2	0.7		
6	NH_2			N	1.1	1.3	0.82	5.4	0.6	>200	

Table 2
Hit optimization. Nine derivatives of the 7-azaindole **7** were tested *in vitro*: compounds **8**–**10** and the six molecules in Table S1. See caption of Table 1 for notes. The PDB codes of the structures of MTH1 in complex with compounds **8** and **9** are 6EQ4 and 6EQ3, respectively.

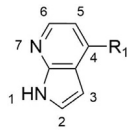

		MTH1				
ID	R1	$IC_{50}(\mu M)$	$K_d(\mu M)$	LE[a]	LLE[c]	ClogP[b]
7	H	132	96	0.59	2.7	1.2
8	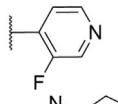	0.8	2.4	0.52	4.2	1.9
9	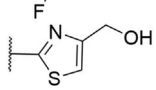	0.4	0.7	0.55	5.7	0.7
10	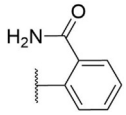	17		0.36	3.5	1.2

hydrogen bond distance (2.8 Å) from the NH_2 group of fragment **6** (Fig. 2A). As a consequence two water molecules are displaced and there is a slight rotation of the plane of the carboxyl group of Asp120. Concerning the hydrogen bonds with the aspartate pair of MTH1, it is interesting to note that the donor-acceptor pattern of our fragment **6** mimics the 6,8-diketo form while the low-nM inhibitor TH588 (5 nM in Ref. 6) mimics the 6-enol-8-keto form of 8-oxo-dGTP (Fig. S10). It has been suggested that MTH1 preferably binds to the 6-enol-8-keto form of 8-oxo-dGTP [10]. The binding of the 6,8-diketo form would require a different protonation state of the Asp-Asp motif of MTH1. Note that modifications of the protonation state of the catalytic dyad upon complex formation have been reported for aspartic proteases [27].

Similar changes in binding pose as for the heterocyclic change between fragment **4** and **6** are unlikely to occur in BACE1 due to the resulting clashes with Asp228 (Fig. 2B). Consistently, in the fluorescence quenching assay we could not measure any inhibition of BACE1 at 200 μM of compound **6** (Fig. S13).

2.2. Molecular dynamics-guided hit optimization

We decided to carry out hit optimization on compound **6** because of its potency and ligand efficiency for MTH1, and its selectivity against BACE1 (Table 1). To validate the pose predicted by docking, which had used a rigid protein structure, we carried out explicit solvent molecular dynamics simulations. The docked pose was stable in five independent runs of 200 ns each (Fig. 3A). The binding site of MTH1 did not show major rearrangements except for an outward rotation of Asn33 (Fig. 3C and D). As a consequence, the hydrogen bonds between fragment **6** and the aspartate pair

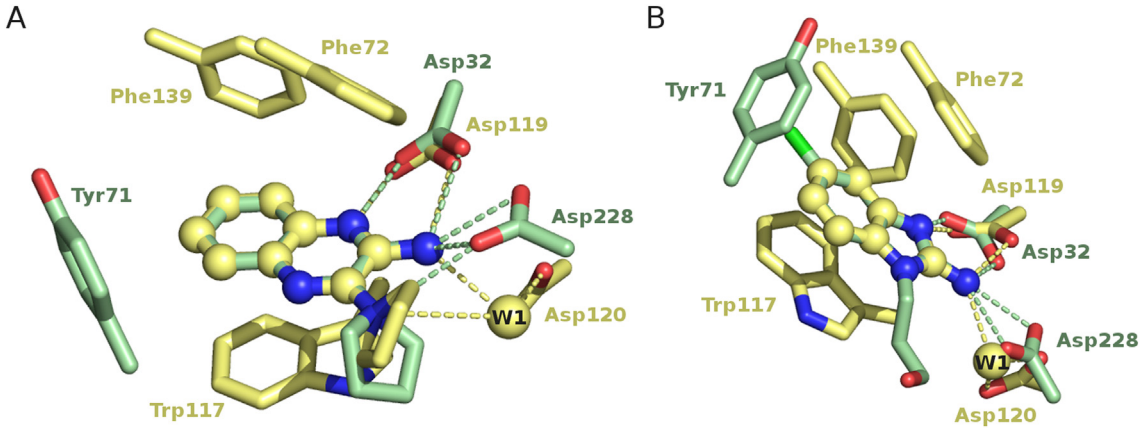

Fig. 1. Ligand retargeting from BACE1 to MTH1. The relative orientation of the two catalytic aspartates in BACE1 (carbon atoms in green) differs slightly from the Asp-Asp pair in MTH1 (yellow). Nevertheless, the binding mode of the retargeted ligands is similar in the two enzymes. (A) Complex of fragment **1** and MTH1 (PDB:6EQ6) overlaid to the complex with BACE1 (PDB:3HW1). (B) Complex of fragment **4** (PDB:6EQ5) and MTH1 overlaid to the complex of fragment **3** and BACE1 (PDB:3MSJ). The crystal structures were overlaid using the atoms in the double-ring systems of the ligands (spheres). The water molecule that bridges the exocyclic NH_2 group and Asp120 in MTH1 is labeled W1 (yellow sphere). Hydrogen bonds to the aspartate pair are shown (dashed lines). (For interpretation of the references to color in this figure legend, the reader is referred to the Web version of this article.)

were stable while those with the Asn33 side chain were broken during most of the sampling (Fig. 3B). In other words, the molecular dynamics results indicate that the interactions with the aspartates contribute more to the affinity than the hydrogen bond to Asn33. Thus, we purchased and tested *in vitro* the 7-azaindole **7** which is the minimal scaffold that can interact with the Asp-Asp pair (Table 2). The favorable ligand efficiency of fragment **7** (0.59 kcal/mol per non-hydrogen atom) validated our molecular dynamics-based hypothesis.

Next, we decided to apply the anchor-based library tailoring (ALTA) procedure [23,28] to improve affinity. We screened *in silico* the nearly 5000 derivatives of fragment **7** that were commercially available. We selected fragment **7** for optimization by catalogue as only 8 and 321 derivatives of fragments **6** and **5**, respectively, were available (Fig. S5). As we wanted to preserve the 7-azaindole core bound to the Asp-Asp motif, we considered derivatives of fragment **7** with substituents at positions 3–6 (see Table 2 for numbering). The docking was carried out using the crystal structures 4C9X and 5ANS which have the outward orientation of the Asn33 side chain and two different orientations of the loop consisting of residues 23–31. Note that the higher flexibility of this loop with respect to the rest of MTH1 had been observed in the molecular dynamics simulations (Fig. S7). Upon docking we discarded compounds in which the 7-azaindole scaffold deviated more than 2 Å from fragment **7**. The remaining compounds were first filtered for a size larger than 15 non-hydrogen atoms to have at least one ring-like substituent. The remaining compounds were sorted according to calculated ligand efficiency (Table S1). From the list of the top 100 compounds we decided to order only nine molecules as they were all available from a single commercial entity (compounds **8**–**10** in Table 2 and **S1-S6** in Table S1). Eight of these compounds at 50 μM concentration showed inhibition of MTH1. Moreover, inhibitor **9** shows sub-micromolar affinity according to both the colorimetric assay and ITC, while inhibitor **8** has an IC_{50} of 0.8 μM in the colorimetric assay and a K_d of 2.4 μM by ITC (Table 2). The three inhibitors **8**–**10** are substituted at position 4 of the 7-azaindole scaffold and the substituents were predicted to occupy the hydrophobic pocket that is filled by the deoxyribose of 8oxo-dGMP. The predicted poses of compounds **8** and **9** were subsequently validated by X-ray crystallography (Fig. S3 and Table S2). Both inhibitors

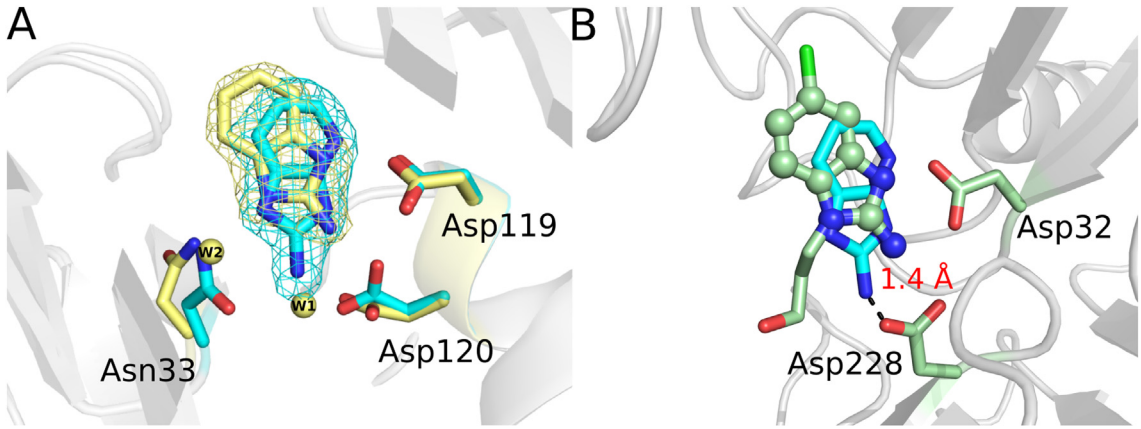

Fig. 2. Different hydrogen bonding-pattern of fragments 4 and 6. (A) The different binding poses of fragments **4** (carbon atoms in yellow, PDB:6EQ5) and **6** (cyan, PDB:6EQ2) are shown with the water molecules in the complex with **4** (spheres). The additional heteroatom in fragment **6** results in displacement of two water molecules and a more buried binding mode than the one of fragment **4**. The 2Fo-Fc maps is contoured at 1σ. The crystal structures were overlaid by using the Cα atoms of the regular elements of secondary structure. (B) The structural overlap of fragment **4** in MTH1 (not shown) and fragment **3** in BACE1 (carbon atoms in green) shows that fragment **6** (cyan) would bump into the side chain of Asp228 of BACE1. (For interpretation of the references to color in this figure legend, the reader is referred to the Web version of this article.)

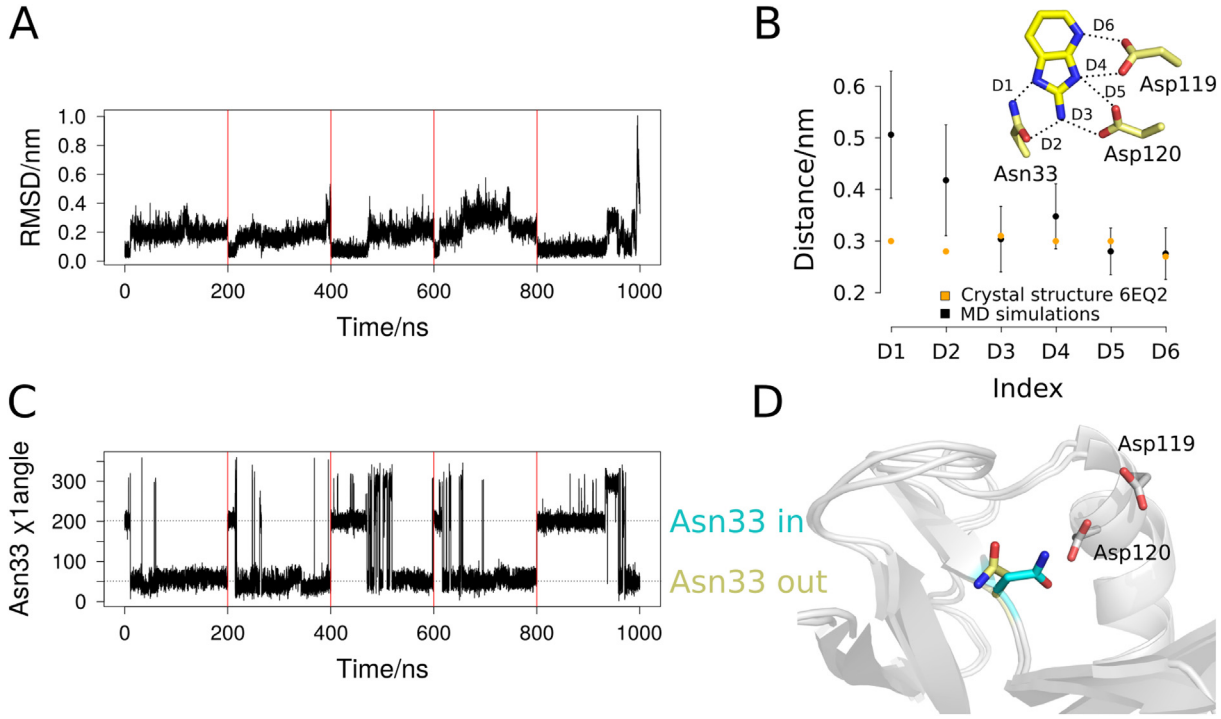

Fig. 3. Stability of docked pose of fragment 6 and interactions with the Asp-Asp motif. (A) The RMSD of fragment **6** in the five 200-ns trajectories (individual runs separated by vertical red line) was calculated by using non-hydrogen atoms and the crystal structure as reference (PDB code 6EQ2). (B) The average distances of the hydrogen bond between fragment **6** and the MTH1 binding site residues. (C) Time series of the χ_1 angle of Asn33 (horizontal lines emphasize the two main orientations of the Asn33 side chain). (D) The two orientations of Asn33 observed in the simulations are shown (colors correspond to those in panel C). (For interpretation of the references to color in this figure legend, the reader is referred to the Web version of this article.)

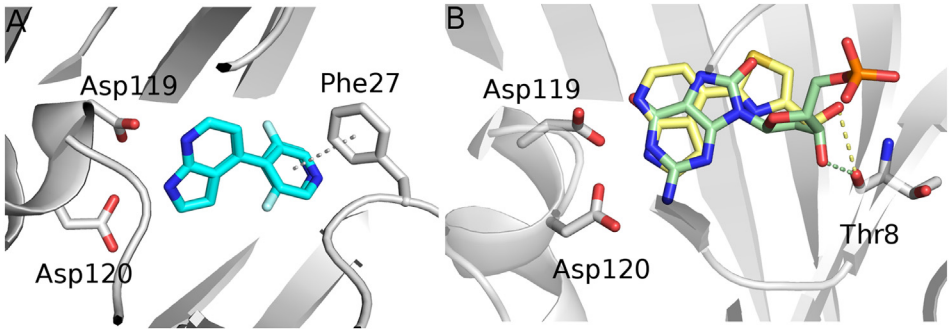

Fig. 4. Crystal structures of MTH1 in the complex with inhibitors 8 and 9. Both inhibitors show the polar interactions with the aspartate pair as predicted by docking. (A) The 3-fluoro-pyridine of inhibitor **8** engages the side chain of Phe27 by an edge-to-face interaction (PDB 6EQ4). Two orientations of fluorine are observed in the electron density map. (B) Structural overlap of MTH1 in complex with 8-oxo-dGMP (carbon atoms in green, PDB 3ZR0) and inhibitor **9** (carbon atoms in yellow, PDB 6EQ3). The Cα atoms of the secondary structure elements of MTH1 were used for the structural overlap. The sulfur atom and nitrogen atom of the thiazole ring of compound **9** occupy the position of the atoms O8 and N9, respectively, of 8-oxo-dGMP. (For interpretation of the references to color in this figure legend, the reader is referred to the Web version of this article.)

retained their 7-azaindole core bound to the Asp-Asp motif (Fig. 4). The 3-fluoro-pyridine of inhibitor **8** is next to the Phe27 in the flexible loop (residues 23–31) which can accommodate different ligands through small changes [9]. The observed edge-to-face π-stacking interaction might contribute to loop stabilization. Interestingly, the superposition of the structures of MTH1 in the complex with the substrate 8oxo-dGMP and inhibitor **9** shows that the sulfur and nitrogen atoms of the thiazole ring overlap with the O8 and N9 atoms of 8oxo-dGMP, respectively (Fig. 4B). In addition, the hydroxyl group of inhibitor **9** is involved in a hydrogen bond with the backbone carbonyl of Thr8 which corresponds to the interaction with the hydroxyl of the deoxyribose.

2.3. Structure-based design of lead compound *11*

The comparison of fragment **7** and its derivative **8** indicate that the 3-fluoro-pyridine of the latter results in a potency improvement by a factor of 40 (according to ITC) to 165 (according to the colorimetry assay) (Table 2). Thus, we hypothesized that the 3-fluoro-pyridine substituent could improve the affinity of the 1 μM fragment hit **6** into the nanomolar range. From the structural alignment of the complexes of MTH1 with fragment **6** and fragment **8** it clearly emerged that the imidazopyridine and 7-azaindole overlap such that the 3-fluoro-pyridine could be substituted in position 7 of the imidazopyridine **6** (Fig. 5A). Thus, we decided to synthesize compound **11** (Fig. 5C and Supplem. Information) which

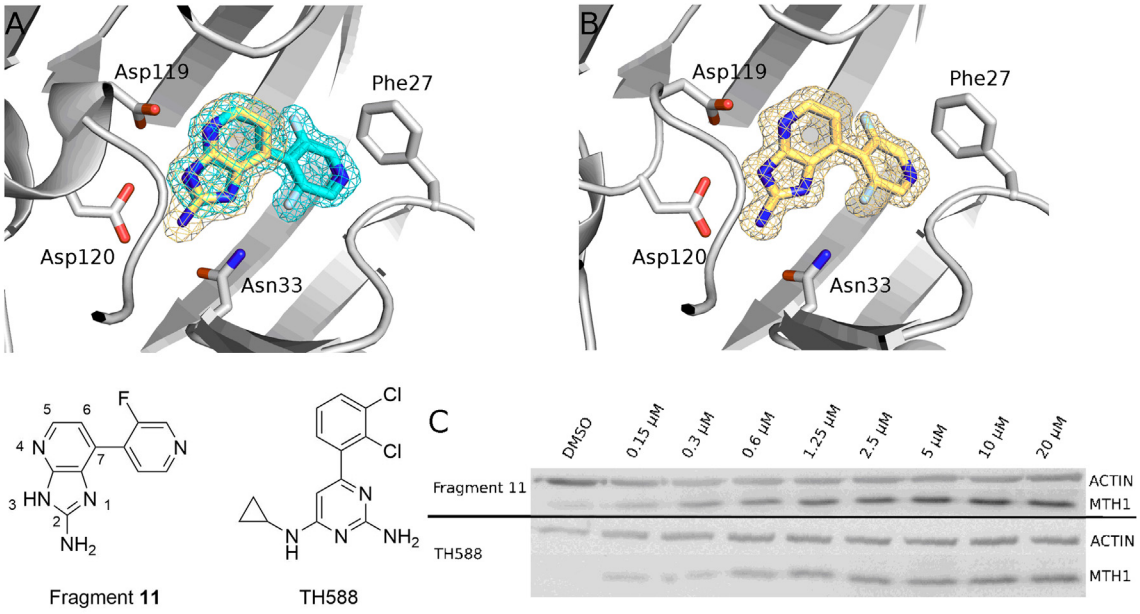

D

	MTH1					BACE1	HeLa
ID	IC_{50} (μM)	K_d (μM)	LE[a]	LLE[c]	ClogP[b]	IC_{50} (μM)	GI_{50} (μM)
11	0.03	0.1	0.61	6.3	1.2	>200	>30
TH588	0.005		0.60	4.1	4.2		3.8

Fig. 5. Design and characterization of the lead compound 11. (A) The overlap of the crystal structures of MTH1 in the complexes with fragment **6** (carbon atoms and electron density in yellow) and fragment **8** (cyan) suggests that the 3-fluoro-pyridine can be substituted also on fragment **6**. The two orientations of the fluorine atom of fragment **8** are shown with the corresponding densities. (B) The crystal structure of the complex of MTH1 and the lead compound **11** validates the design. (C) Chemical structures and CETSA results. In the absence of inhibitors, MTH1 unfolds and precipitates at high temperature (> 58°C) in K562 cells. The inhibitors stabilize MTH1 and raise the melting temperature. The amount of unprecipitated protein was quantified by Western Blot. The nanomolar inhibitor TH588 (5 nM in Ref. 6) was used as positive control. (D) The values of affinity of our lead **11** and the inhibitor TH588 in binding assays with recombinant MTH1 are tabulated (see caption of Table 1 for notes), together with the cytotoxic effect on HeLa cells. (For interpretation of the references to color in this figure legend, the reader is referred to the Web version of this article.)

was not commercially available. Note that we also considered to decorate the fragment hit **6** in position 7 with the thiazole substitution instead of the 3-fluoro-pyridine but realized that its synthesis would be more difficult than the one of compound **11**. The crystal structure of the complex with compound **11** validates our structure-based design as its imidazopyridine and 3-fluoro-pyridine occupy the same position and are involved in the same interactions as fragment **6** and the 3-fluoro-pyridine of compound **8**, respectively (Fig. 5A and B). As already observed for fragment **8**, the fluorine atom on the pyridine ring points either to the Asn33 or to the opposite hydrophobic site consisting of Ile70, Phe72, Met81, and Val83. Gratifyingly compound **11** shows an IC_{50} of 0.03 μM in the colorimetric assay and a K_d of 0.1 μM by ITC (Fig. 5D). Furthermore, the selectivity of our lead **11** against BACE1 and hERG is higher than a factor of 2000 as lead **11** at 200 μM does not show inhibition of these off-targets (Figs. S13 and S14). A potential hERG liability was investigated as the optimization program of fragment **3** on BACE1 resulted in a series of inhibitors that block hERG [29].

We checked our inhibitors for potential assay interference and/or aggregation. The compounds **1**–**11** were negative in tests for known pan-assay interference (PAINS) substructures at the FAF-Drugs4 Web server [30]. Furthermore, except for fragments **3** and **5**, our inhibitors are negative in a test for known aggregation substructures or properties at the Aggregator Advisor Web server [31]. A potential aggregation of fragment **3** was not reported in Ref. 29 in which it was selected as starting scaffold for an inhibitor series to target BACE1. Fragment **5** is similar to part of an aromatic four-ring system (Fig. S8) and because of its smaller size it is likely not to be problematic. The use of ITC as a complementary and orthogonal binding assay excludes possible assay interferences of compounds with the colorimetric assay. Moreover, the direct measurement of ligand-protein binding by ITC (Fig. S11) provides further evidence of one to one binding to MTH1.

Next we decided to assess the activity of our lead compound in the cell with a target-engagement assay. For this purpose, **11** was tested in a cellular thermal shift assay (CETSA) which monitors the increase in thermal stability upon ligand binding. The stabilization of MTH1 as measured by CETSA is evident already at sub-micromolar concentrations of **11** (Fig. 5C) which is consistent with the nanomolar potency measured by ITC and in the colorimetric assay.

To evaluate its potential as anticancer lead compound, fragment **11** was tested on HeLa cells by resazurin-based cell proliferation assay using TH588 as a positive control. Although both TH588 and our lead compound **11** show nanomolar potency in the MTH1 enzymatic assay (Fig. S12) and CETSA (Fig. 5C), only TH588 showed antiproliferative effects in HeLa cells. The GI_{50} of 3.8 μM (Fig. S15) measured for TH588 is in good agreement with the published value of 2.6 μM [6]. Thus, our CETSA and cell-proliferation assays provide further evidence that the cytotoxic activity of TH588 originates from off-target effects as reported in recent studies [8,9].

Irrespective of the validity of MTH1 as a drug target, our strategy of retargeting BACE1 inhibitors for MTH1, which is based on the common pair of aspartate residues, resulted in efficient hit finding and follow-up optimization. The same strategy can be applied to other pairs of non-homologus enzymes (or receptors) that have analogous binding sites.

3. Conclusions

We have hypothesized that similarity in the binding sites of two unrelated enzymes can be exploited for ligand identification. Following our hypothesis we have screened 342 inhibitors of aspartic proteases for binding to MTH1 as MTH1 features a pair of aspartates adjacent to its catalytic site. The screening was carried out by docking and yielded three fragment hits with very favorable ligand efficiency. Molecular dynamics simulations provided information on the key interactions of the 1-μM hit **6**. These interactions were preserved during hit optimization in the space of commercially available compounds. The overlap of the crystal structures of MTH1 in the complexes with fragment **6** and compound **8** suggested the synthesis of compound **11**. The structure-based design was successful as the lead compound **11** shows nanomolar potency for MTH1 and high selectivity against the potential off-targets BACE1 and hERG. The predicted binding modes of five compounds were validated by protein crystallography which provides evidence that structural analogy can be exploited for (*in silico*) ligand identification. Ligand retargeting by binding site analogy is particularly useful for those targets that show structural analogy with binding sites of unrelated proteins for which many inhibitors are known.

Funding

This work was supported by a grant of the Swiss National Science Foundation [31003A_169007, to AC] and a predoctoral fellowship of the Forschungskredit of the University of Zurich [FK-16-032, to LW].

Acknowledgement

We thank the staff at beamlines X06SA and X06DA of the Swiss Light Source (SLS, PSI Villigen). We thank Stefanie Eberle for helping in performing some ITC measurements. We also thank T. Hettich from the FHNW University of Applied Sciences and Arts Northwestern Switzerland for carrying out the LC-MS experiments. We are grateful to Thomas Helleday (Karolinska Institutet, Stockholm) for providing the expression construct of MTH1. We thank Vlad Pascanu for technical support with compound **2**.

Appendix A. Supplementary data

Supplementary data to this article can be found online at https://doi.org/10.1016/j.ejmech.2019.04.037.

References

[1] Y. Nakabeppu, Molecular genetics and structural biology of human MutT homolog, MTH1, Mutat. Res. 477 (2001) 59–70.
[2] A. Kumar, T. Kawamura, M. Kawatani, H. Osada, K.Y.J. Zhang, Identification and structure-activity relationship of purine derivatives as novel MTH1 inhibitors, Chem. Biol. Drug Des. 89 (2017) 862–869.
[3] M. Muroi, Y. Kondoh, Y. Futamura, H. Aono, M. Tanaka, K. Honda, H. Osada, Proteomic profiling of small-molecule inhibitors reveals dispensability of MTH1 for cancer cell survival, Sci. Rep. 6 (2016) 26521.
[4] F. Rahm, et al., Creation of a novel class of potent and selective MutT homologue 1 (MTH1) inhibitors using fragment-based screening and structure-based drug design, J. Med. Chem. 61 (2018) 2533–2551.
[5] A. Rudling, R. Gustafsson, I. Almlöf, E. Homan, M. Scobie, U. Warpman Berglund, T. Helleday, P. Stenmark, J. Carlsson, Fragment-based discovery and optimization of enzyme inhibitors by docking of commercial chemical space, J. Med. Chem. 60 (2017) 8160–8169.
[6] H. Gad, et al., MTH1 inhibition eradicates cancer by preventing sanitation of the dNTP pool, Nature 508 (2014) 215–221.
[7] K.V.M. Huber, et al., Stereospecific targeting of MTH1 by (S)-crizotinib as an anticancer strategy, Nature 508 (2014) 222–227.
[8] M. Ellermann, et al., Novel class of potent and cellularly active inhibitors devalidates MTH1 as broad-spectrum cancer target, ACS Chem. Biol. 12 (2017) 1986–1992.
[9] J.G. Kettle, et al., Potent and selective inhibitors of MTH1 probe its role in cancer cell survival, J. Med. Chem. 59 (2016) 2346–2361.
[10] L.M. Svensson, A.-S. Jemth, M. Desroses, O. Loseva, T. Helleday, M. Högbom, P. Stenmark, Crystal structure of human MTH1 and the 8-oxo-dGMP product complex, FEBS Lett. 585 (2011) 2617–2621.
[11] H.M. Berman, J. Westbrook, Z. Feng, G. Gilliland, T.N. Bhat, H. Weissig, I.N. Shindyalov, P.E. Bourne, The protein data bank, Nucleic Acids Res. 28 (2000) 235–242.
[12] Y. Hamada, Y. Kiso, New directions for protease inhibitors directed drug discovery, Biopolymers 106 (2016) 563–579.
[13] J. Eder, U. Hommel, F. Cumin, B. Martoglio, B. Gerhartz, Aspartic proteases in drug discovery, Curr. Pharmaceut. Des. 13 (2007) 271–285.
[14] S. Pérot, O. Sperandio, M.A. Miteva, A.-C. Camproux, B.O. Villoutreix, Druggable pockets and binding site centric chemical space: a paradigm shift in drug discovery, Drug Discov. Today 15 (2010) 656–667.
[15] A. Macchiarulo, R. Pellicciari, Exploring the other side of biologically relevant chemical space: insights into carboxylic, sulfonic and phosphonic acid bioisosteric relationships, J. Mol. Graph. Model. 26 (2007) 728–739.
[16] A. Macchiarulo, R. Nuti, G. Eren, R. Pellicciari, Charting the chemical space of target sites: insights into the binding modes of amine and amidine groups, J. Chem. Inf. Model. 49 (2009) 900–912.
[17] S. Ruiz-Carmona, D. Alvarez-Garcia, N. Foloppe, A.B. Garmendia-Doval, S. Juhos, P. Schmidtke, X. Barril, R.E. Hubbard, S.D. Morley, rDock: a fast, versatile and open source program for docking ligands to proteins and nucleic acids, PLoS Comput. Biol. 10 (2014) e1003571.
[18] J.W.M. Nissink, M. Bista, J. Breed, N. Carter, K. Embrey, J. Read, J.J. Winter-Holt, MTH1 substrate recognition—an example of specific promiscuity, PLoS One 11 (2016) e0151154.
[19] B.R. Brooks, et al., CHARMM: the biomolecular simulation program, J. Comput. Chem. 30 (2009) 1545–1614.
[20] R.B. Best, X. Zhu, J. Shim, P.E.M. Lopes, J. Mittal, M. Feig, A.D. Mackerell, Optimization of the additive CHARMM all-atom protein force field targeting improved sampling of the backbone φ, ψ and side-chain $\chi(n)$ and $\chi(2)$ dihedral angles, J. Chem. Theory Comput. 8 (2012) 3257–3273.
[21] K. Vanommeslaeghe, A.D. MacKerell, Automation of the CHARMM General Force Field (CGenFF) I: bond perception and atom typing, J. Chem. Inf. Model. 52 (2012) 3144–3154.
[22] W. Im, D. Beglov, B. Roux, Continuum solvation model: computation of electrostatic forces from numerical solutions to the Poisson-Boltzmann equation, Comput. Phys. Commun. 111 (1998) 59–75.
[23] J.-R. Marchand, A. Dalle Vedove, G. Lolli, A. Caflisch, Discovery of inhibitors of four bromodomains by fragment-anchored ligand docking, J. Chem. Inf. Model. 57 (2017) 2584–2597.
[24] M. Cecchini, P. Kolb, N. Majeux, A. Caflisch, Automated docking of highly flexible ligands by genetic algorithms: a critical assessment, J. Comput. Chem. 25 (2004) 412–422.
[25] J.-R. Marchand, A. Caflisch, In silico fragment-based drug design with SEED, Eur. J. Med. Chem. 156 (2018) 907–917.
[26] P.J. Hajduk, J. Greer, A decade of fragment-based drug design: strategic advances and lessons learned, Nat. Rev. Drug Discov. 6 (2007) 211–219.
[27] F. Sussman, M.C. Villaverde, J. Dominguez, U.H. Danielson, On the active site protonation state in aspartic proteases: implications for drug design, Curr. Pharmaceut. Des. 19 (2013) 4257–4275.
[28] P. Kolb, C.B. Kipouros, D. Huang, A. Caflisch, Structure-based tailoring of compound libraries for high-throughput screening: discovery of novel EphB4 kinase inhibitors, Proteins 73 (2008) 11–18.
[29] J. Madden, J.R. Dod, R. Godemann, J. Kraemer, M. Smith, M. Biniszkiewicz, D.J. Hallett, J. Barker, J.D. Dyekjaer, T. Hesterkamp, Fragment-based discovery and optimization of BACE1 inhibitors, Bioorg. Med. Chem. Lett 20 (2010) 5329–5333.
[30] D. Lagorce, O. Sperandio, J.B. Baell, M.A. Miteva, B.O. Villoutreix, FAF-Drugs3: a web server for compound property calculation and chemical library design, Nucleic Acids Res. 43 (2015) W200–W207.
[31] J.J. Irwin, D. Duan, H. Torosyan, A.K. Doak, K.T. Ziebart, T. Sterling, G. Tumanian, B.K. Shoichet, An aggregation advisor for ligand discovery, J. Med. Chem. 58 (2015) 7076–7087.
[32] R. Godemann, J. Madden, J. Krämer, M. Smith, U. Fritz, T. Hesterkamp, J. Barker, S. Höppner, D. Hallett, A. Cesura, A. Ebneth, J. Kemp, Fragment-based discovery of BACE1 inhibitors using functional assays, Biochemistry 48 (2009) 10743–10751.
[33] A. Kuglstatter, M. Stahl, J.-U. Peters, W. Huber, M. Stihle, D. Schlatter, J. Benz, A. Ruf, D. Roth, T. Enderle, M. Hennig, Tyramine fragment binding to BACE-1, Bioorg. Med. Chem. Lett 18 (2008) 1304–1307.